

1 **Climate-Driven Shifts in Continental Net Primary**  
2 **Production Implicated as a Driver of a Recent Abrupt**  
3 **Increase in the Land Carbon Sink**

4 **W. Buermann<sup>1</sup>, C. Beaulieu<sup>2</sup>, B. Parida<sup>3</sup>, D. Medvigy<sup>4</sup>, G.J. Collatz<sup>5</sup>,**  
5 **J. Sheffield<sup>6</sup>, and J.L. Sarmiento<sup>4</sup>**

6

7 <sup>1</sup>Institute for Climate and Atmospheric Science, School of Earth and Environment,  
8 University of Leeds, Leeds LS2 9JT, UK.

9 <sup>2</sup>Ocean and Earth Science, National Oceanography Centre Southampton  
10 University of Southampton, Southampton SO14 3ZH, UK

11 <sup>3</sup>Civil Engineering Department, Shiv Nadar University, Dadri, 203207 UP, India

12 <sup>4</sup>Atmospheric and Oceanic Sciences Program, Princeton University, 08540 Princeton,  
13 New Jersey, USA.

14 <sup>5</sup>National Aeronautics and Space Administration, Goddard Space Flight Center, 20771  
15 Greenbelt, Maryland, USA.

16 <sup>6</sup>Department of Civil and Environmental Engineering, Princeton University, 08540  
17 Princeton, New Jersey, USA.

18

19

20 Correspondence to W. Buermann (w.buermann@leeds.ac.uk)

21

22

1 **Abstract**

2 The World's ocean and land ecosystems act as sinks for anthropogenic CO<sub>2</sub>, and over the  
3 last half century their combined sink strength grew steadily with increasing CO<sub>2</sub>  
4 emissions. Recent analyses of the global carbon budget, however, uncovered an abrupt,  
5 substantial (~1 PgC yr<sup>-1</sup>) and sustained increase in the land sink in the late 1980s whose  
6 origin remains unclear. In the absence of this prominent shift in the land sink, increases in  
7 atmospheric CO<sub>2</sub> concentrations since the late 1980s would have been ~30% larger than  
8 observed (or ~12 ppm above current levels). Global data analyses are limited in regards  
9 to attributing causes to changes in the land sink because different regions are likely  
10 responding to different drivers. Here, we address this challenge by using terrestrial  
11 biosphere models constrained by observations to determine if there is independent  
12 evidence for the abrupt strengthening of the land sink. We find that net primary  
13 production has significantly increased in the late 1980s (more so than heterotrophic  
14 respiration) consistent with the inferred increase in the global land sink, and that large-  
15 scale climate anomalies are responsible for this shift. We identify two key regions in  
16 which climatic constraints on plant growth have eased: northern Eurasia experienced  
17 warming, and northern Africa received increased precipitation. Whether these changes in  
18 continental climates are connected is uncertain, but North Atlantic climate variability is  
19 important. Our findings suggest that improved understanding of climate variability in the  
20 North Atlantic may be essential for more credible projections of the land sink under  
21 climate change.

# 1 **1 Introduction**

2 The world's land ecosystems act as a major sink in the contemporary global carbon cycle  
3 and, hence, alleviates the rise of atmospheric CO<sub>2</sub> concentrations from global CO<sub>2</sub>  
4 emissions and as a consequence climate change (IPCC, 2013). Yet, while critical for  
5 society our present understanding of the evolution of the land carbon sink under global  
6 change is still severely limited (Le Quéré et al., 2009). This is in part because multiple  
7 complex factors can influence the carbon balance of terrestrial ecosystems, including  
8 climate change, land-use and land-cover change (forest regrowth, fire suppression etc.),  
9 nitrogen deposition, and CO<sub>2</sub> fertilization (Ciais et al., 2013). In this regard, it has been  
10 well documented that the land carbon sink (typically inferred as the 'residual' in the  
11 global carbon mass balance of fossil fuel and net land use change (LUC) emissions, the  
12 atmospheric CO<sub>2</sub> growth rate and oceanic uptake) is quite variable at decadal time scales  
13 (Denman et al., 2007). But, in recent global carbon budget (GCB) studies with longer (~  
14 last 5 decades) and annually resolved records a rather abrupt, substantial (~1 PgC yr<sup>-1</sup>)  
15 and sustained strengthening of the 'residual' land carbon sink in the late 1980s has been  
16 identified (Sarmiento et al., 2010; Beaulieu et al., 2012). Our overall confidence in this  
17 prominent shift, however, is somewhat limited since the 'residual' land sink is the most  
18 uncertain term in the GCB. This is because uncertainties embedded in the individual  
19 budget terms (e.g. LUC emissions and oceanic uptake) propagate into estimates of the  
20 'residual' land carbon sink (Le Quéré et al., 2013).

21 Here, we explore if there is further independent evidence for a late 1980s regime  
22 shift in the land carbon sink through analyzing carbon fluxes from biospheric models of  
23 various complexity and observational constraints (e.g. satellite-based vegetation activity).

1 Our emphasis is on global pattern of net primary production (NPP) since this key carbon  
2 flux is known to be a robust driver of carbon sink variability (Luysaert et al., 2007; Zhao  
3 and Running, 2010). A particular focus is in identifying which land regions may have  
4 contributed to the potential shift and what underlying mechanisms may have caused it.  
5 Specifically, we analyze data-driven NPP data based on an established satellite-  
6 constrained biogeochemical model as well as process-based NPP data from nine  
7 terrestrial biosphere models that participated in a recent model intercomparison project  
8 ‘trends and drivers of the regional-scale sources and sinks of carbon dioxide (TRENDY)’  
9 (Section 2).

10

## 11 **2 Methods**

### 12 **2.1 Data and models**

13 We analyze temporal patterns in various metrics of the terrestrial carbon cycle based on  
14 three independent data sources. First, we analyze data-driven NPP fields based on  
15 simulations with the satellite-constrained biogeochemical Carnegie-Ames-Stanford-  
16 Approach (CASA) model (van der Werf et al., 2006) for the period of available satellite  
17 vegetation data 1982-2011 (Zhu et al., 2013). This updated and extensively validated  
18 model runs at a 0.5° spatial resolution on a monthly time step. NPP is a measure of the  
19 amount of carbon fixed by plants during photosynthesis and accumulated as biomass. The  
20 CASA model is conceptually relative simple and a number of potentially important  
21 processes and mechanisms, such as related to nutrients (e.g., carbon and nitrogen) are not  
22 considered explicitly (van der Werf et al., 2006). However, factors that influence  
23 vegetation productivity may be indirectly captured through the satellite-based fraction of

1 available photosynthetically active radiation absorbed by plants (fAPAR), a key driver in  
2 the NPP CASA light use efficiency parameterization (van der Werf et al., 2006). This is  
3 demonstrated by two recent studies showing that trends in satellite-based vegetation  
4 cover are consistent with expectations of growth enhancement via the CO<sub>2</sub> fertilization  
5 effect (Donohue et al., 2013; Los, 2013). Yet there is also new evidence suggesting that  
6 in dense forested ecosystems (tropical rainforests) fAPAR may not be fully responsive to  
7 the CO<sub>2</sub> fertilization effect (Forkel et al. 2015). Temporally varying driver data used for  
8 the CASA simulations include in addition to satellite-based fAPAR (fAPAR3g) (Zhu et  
9 al., 2013) also land temperature (CRU TS3.21) (Harris et al., 2014) as well as  
10 precipitation and surface solar radiation. We pay particular attention to uncertainties in  
11 these observational-based datasets and corresponding effects on NPP estimates. While  
12 land surface temperature data are considered to be relatively robust, a substantial  
13 limitation is that presently only one consistent satellite fAPAR dataset exists that covers  
14 the last 3 decades (Zhu et al., 2013) which we consider a minimum record length for  
15 meaningful change point analysis. Nonetheless, to account at least partially for  
16 observational uncertainties we evaluated different data sources for precipitation and  
17 surface solar radiation which are known to have substantial uncertainties (Wild, 2009;  
18 Greve et al., 2014) (see Methods in the Supplement). Based on a final selection of driver  
19 datasets (1 fAPAR, 1 temperature, 3 precipitation and 3 solar radiation; see Table S4 in  
20 the Supplement) we performed multiple CASA simulations with all possible input  
21 combinations (a total of 9 simulations) and analyzed the NPP ensemble mean with our  
22 change point methodology. We used the spread in these simulations as a measure of  
23 ‘observational-based’ uncertainty. In a complementary analysis, we also analyzed the

1 heterotrophic respiration ( $R_h$ ) and net ecosystem production (NEP; estimated as  $NPP -$   
2  $R_h$ ) ensemble means from these sets of CASA simulations. To ensure that the carbon  
3 pools are at steady state, the CASA model was spun up for 250 years using a driver  
4 climatology based on the study period 1982-2011.

5 Second, we analyze a GCB for the period 1959-2011 and consisting of  $CO_2$   
6 emissions from fossil fuel burning and cement production as well as net LUC emissions,  
7 atmospheric  $CO_2$  growth rates and oceanic uptake (Le Quéré et al., 2013). Uncertainties  
8 in these budget terms are also provided and utilized to estimate uncertainties in net land  
9 uptake and the residual land sink (through the sum of squared errors).

10 Third, we analyze process-based  $NPP$ ,  $R_h$  and NEP data based on ensembles of  
11 nine single terrestrial biosphere models that participated in the recent TRENDY model  
12 intercomparison project (Sitch et al., 2015). Compared to CASA, the TRENDY models  
13 are substantially more complex and also run at significantly shorter time steps to resolve  
14 the diurnal cycle needed when coupled within Earth system climate models (Sitch et al.,  
15 2015). An important distinction is that in the TRENDY models vegetation characteristics  
16 (e.g. fAPAR) are simulated prognostically (unlike in CASA where such information is  
17 inferred from satellite observations). In the TRENDY experiments (Sitch et al., 2015) the  
18 models were driven with observed climate and atmospheric  $CO_2$  data (S2 experiments) as  
19 well as with observed atmospheric  $CO_2$  data only (S1) and in order to isolate the  
20 variability due to climate, the difference between these two experiments (S2 – S1) was  
21 taken. We analyze the  $NPP$ ,  $R_h$  and NEP ensemble means (based on anomalies) from the  
22 nine participating models (Community Land Model 4CN, Hyland, Lund-Potsdam-Jena  
23 (LPJ), LPJ-GUESS, ORCHIDEE, Sheffield-DGVM, TRIFFID and VEGAS; for model

1 details see Sitch et al., 2015) and used the spread among them as a measure of ‘model-  
2 based’ uncertainty in our change point framework. Based on a recent comprehensive  
3 evaluation against observations, it was found that most of the TRENDY models are  
4 capable of simulating the short- and long-term first-order dynamics of the terrestrial  
5 carbon cycle (Piao et al., 2013).

6

## 7 **2.2 Statistical methodology**

8 We apply a consistent change point methodology on the various metrics of the terrestrial  
9 carbon cycle to identify pattern of regime shifts (characterized as abrupt, substantial and  
10 sustained changes) and to contrast them to pattern showing either no or more gradual  
11 changes. We thus determine in a first step the statistical model that best fits the time  
12 series under investigation based on three options: 1) a constant mean, 2) a shift in the  
13 mean and 3) a linear trend. While there are numerous alternative statistical models (e.g.  
14 shifting trends as seen in satellite vegetation data at local to regional scales  
15 (Piao et al., 2011)), our choice of these three models is based on our primary objective to  
16 identify large-scale pattern in global and continental carbon fluxes that would be  
17 consistent with the recently observed regime shift in the land carbon sink (Sarmiento et  
18 al., 2010; Beaulieu et al., 2012).

19 In the ‘shift in the mean’ model, the shift is located through a change point  
20 detection algorithm that includes discrimination against a trend and the background  
21 autocorrelation (red noise) by considering all positions in a time series as a potential  
22 change point from 5 to  $n-5$ , with  $n$  being the record length (Beaulieu et al. 2012b). In a  
23 previous study, we found that by restricting the search for change points in this manner

1 detection of spurious shifts at the beginning or end of a series can be avoided  
2 (Beaulieu et al. 2012a). In the change point method applied here, we also further  
3 developed the Beaulieu et al. (2012b) methodology to account for known explicit  
4 uncertainties in the time series under investigation. One important limitation here is that  
5 this statistical change point model cannot distinguish between a rather drastic shift (e.g.,  
6 change from one year to the next) and a more smooth shift over the span of several years.  
7 Adding additional parameters could in principle provide more information on the nature  
8 of the shift (e.g., smooth versus abrupt) but this would also make the model prone to  
9 overfitting given the rather short time series in this study.

10       The most likely model among the three statistical models fitted is determined  
11 based on the Schwarz Information Criterion (SIC), which compares their likelihoods with  
12 a penalty for the number of parameters fitted. If the ‘shift in the mean’ model seems the  
13 most likely, we calculate in a second step the direction and magnitude of the shifts  
14 (subtracting means prior and after the shift) and the corresponding *P*-value by integrating  
15 the full uncertainty of the data using Monte Carlo simulations. To perform the Monte  
16 Carlo simulation, we draw 1000 normally distributed synthetic series having the same  
17 statistical properties as the time series of interest. A new feature is that the series are  
18 simulated with uncertainty additivity: the squared variance of each data point is added to  
19 the overall time series squared variance and the square root of this sum provides the  
20 synthetic series variance. This therefore takes into account the explicit uncertainties in the  
21 various time series under investigation. The change point method is applied to the  
22 synthetic time series and a SIC difference between the model with a shift in the mean and  
23 no shift is calculated for each time series. This provides a distribution for the SIC

1 difference under the hypothesis of no shift in the mean. The  $P$ -value is the estimated  
2 probability to find a SIC difference at least as extreme as the one observed, under the  
3 hypothesis of no change. This methodology assumes that the errors of the model are  
4 independent and normally distributed with a constant variance. We test normality of the  
5 residuals using the Lilliefors test, the independence is verified using the Durbin-Watson  
6 test and the constant variance is verified using a Fisher test. All tests are available and  
7 performed using MATLAB. If independence is not respected, we generate synthetic  
8 series with the same first-order autocorrelation as observed in the respective time series  
9 residuals.

10

## 11 **3 Results**

### 12 **3.1 Shifts in data-driven NPP**

13 Applying our change point methodology (Section 2.2) on data-driven global NPP fields  
14 reveals a marked spatial clustering of abrupt and sustained increases in NPP across  
15 northern Eurasia and northern Africa in the late 1980s (Fig. 1). At more regional levels,  
16 the impact of severe disturbance events such as the mountain pine beetle outbreak in the  
17 late 1990s in the temperate and boreal forests of western North America  
18 (Kurz et al., 2008) is also disclosed (via rapid and sustained decreases in NPP). A similar  
19 analysis without constraining to only statistically significant results at the grid point level  
20 implies that the coherent pattern of abrupt and sustained NPP shifts across northern  
21 Eurasia and northern Africa are spatially even more extensive (Fig. S1 in the  
22 Supplement).

23 This point is further illustrated when we apply our change point framework on

1 data-driven NPP time series representative of large land regions and highlights the  
2 important role of the northern extratropics (magnitude of NPP shift:  $\sim 0.7 \text{ PgC yr}^{-1}$ ), and  
3 the northern Eurasian continent ( $\sim 0.5 \text{ PgC yr}^{-1}$ ) in particular, in the regime shift in carbon  
4 uptake by terrestrial plants in the late 1980s (Table 1 and Fig. S2 in the Supplement).  
5 While the northern African region also exhibits a robust albeit smaller increase in data-  
6 driven NPP ( $\sim 0.2 \text{ PgC yr}^{-1}$ ) in the late 1980s, no corresponding NPP shifts are  
7 discernable for tropical/southern and global land areas (Table 1). It is well known that  
8 factors like ENSO (van der Werf et al., 2004) and volcanic aerosols (Lucht et al., 2002)  
9 have a large influence on variability in the carbon balance of terrestrial ecosystems  
10 (particularly at interannual time scales) and these phenomena may have also played a role  
11 in the prominent late 1980s NPP regime shifts. An analysis that explicitly accounts for  
12 such effects however suggests that these two factors are not the causes of the shift, but  
13 indicates that a shift in data-driven NPP in the late 1980s emerges also for  
14 tropical/southern and global land regions albeit with limited statistical significance  
15 (Table 1). In a complementary analysis, we also re-assessed the robustness of the earlier  
16 reported abrupt shift in the ‘residual’ global land carbon sink in the late 1980s (Sarmiento  
17 et al., 2010; Beaulieu et al., 2012a) by analyzing a GCB for the period 1959-2011 (Le  
18 Quéré et al., 2013) with our change point methodology that also accounts for explicit  
19 uncertainties in the individual budget terms (Section 2.2). Results confirm the presence of  
20 a regime shift in the global ‘residual’ land sink ( $\sim 1\text{-}1.3 \text{ PgC yr}^{-1}$  depending on statistical  
21 treatment) in the late 1980s (Table 1 and Fig. S3 in the Supplement). Taken together, the  
22 good agreement in the timing of regime shifts in the global ‘residual’ land carbon sink  
23 and continental data-driven NPP may imply that the latter is a significant driver of the

1 increased terrestrial carbon uptake in the late 1980s.

2

### 3 **3.2 Drivers of the late-1980s shift in data-driven NPP**

4 In order to unravel the mechanisms leading to the continental shifts in data-driven NPP,  
5 we focus on the two target regions of northern Eurasia and northern Africa that  
6 predominantly contributed to this late 1980s shift (see Fig. 1a). A factorial analysis for  
7 specific seasons shows that the northern Eurasian continent experienced a marked  
8 increase in spring temperatures and spring satellite vegetation activity (fAPAR) in the  
9 late 1980s that together drove a substantial increase in spring NPP (Fig. 2a). This  
10 relatively sudden springtime warming was also associated with a marked earlier spring  
11 onset (~5 days; see Fig. S4 in the Supplement) and the enhanced productivity in the early  
12 part of the growing season appears to have also benefited plant productivity in  
13 subsequent summers (Fig. 2a and Fig. S4 in the Supplement). Increased plant  
14 productivity in both of these seasons contributed predominantly to the pronounced and  
15 sustained increases in annual NPP in the late 1980s (Fig. 2a). Over northern Africa  
16 including the dry Sahel, marked increases in data-driven NPP during wet and dry seasons  
17 that are driven by both increases in rainfall as well as satellite fAPAR triggered a  
18 pronounced increase in annual NPP in the late 1980s (Fig. 2b). A closer inspection shows  
19 that in the period after this shift rainfall increased specifically during the later portion of  
20 the rainy season, which effectively lengthened the more productive growing season  
21 (Fig. S4 in the Supplement).

22

### 23 **3.3 Shifts in process-based NPP**

1 The exploited biogeochemical model (CASA) for data-driven NPP simulations has a  
2 relatively simple structure and provides an integrated view (via satellite fAPAR) of the  
3 many interacting factors that influence NPP variability. Further, data-driven NPP  
4 estimates are also influenced by observational uncertainties in both satellite (e.g.,  
5 volcanic aerosols, cloud cover, signal saturation) and key climate driver data that are only  
6 partially accounted for in our data-driven NPP simulations (see Section 2.1). We thus  
7 explored if process-based terrestrial biosphere models driven by climate and atmospheric  
8 CO<sub>2</sub> observations also show evidence of a marked shift in NPP in the late 1980s. Results  
9 based on the TRENDY ensembles (Section 2) show that for the satellite period (~ last 3  
10 decades) a NPP shift in the late 1980s emerges as a prominent feature, but only in  
11 experiments that capture variability due to climate exclusively (Fig. 3, Fig. S5 and Table  
12 S1 in the Supplement). Regional attributions associated with the shift are similar as in the  
13 case for data-driven NPP, but differences in NPP sensitivities to climate (inferred from  
14 differences in the magnitude of the shifts) are evident (Table 1 and Table S1 in the  
15 Supplement). For example, the magnitude of the late 1980s NPP shift in Northern Eurasia  
16 based on TRENDY is only about half the size of the corresponding shift in data-driven  
17 NPP (Table 1 and Table S1 in the Supplement). One reason for this marked difference  
18 may be that seasonal carry-over effects in NPP are largely absent in the TRENDY  
19 models; e.g. the late 1980s Northern Eurasian annual NPP shift in TRENDY is solely due  
20 to spring contributions (coincident with the time of the climate forcing) whereas for data-  
21 driven NPP it is comprised of about equal contributions from spring and summer (Figs 2a  
22 and 3a). It should be noted that such seasonal carry-over effects due to an earlier spring  
23 onset are indeed observed at multiple eddy covariance flux sites across temperate and

1 boreal ecosystems (Richardson et al., 2010) and that the phenology response (at seasonal  
2 and interannual time scales) in data-driven approaches is generally considered more  
3 robust (Raczka et al., 2013).

4 The TRENDY simulations are not restricted to the satellite period allowing us to  
5 assess whether the identified late 1980s NPP shifts also emerge as dominant pattern when  
6 the study period is extended to the last 5 decades (to be consistent with the time frame of  
7 the GCB). Results show that the late 1980s shift over northern Eurasia is a stable pattern.  
8 For northern Africa, however, an even more prominent shift is identified in the late 1960s  
9 (Fig. S5 and Table S1 in the Supplement). This may suggest that this region by itself is  
10 not important enough to influence the global land sink (since there is no evidence for a  
11 corresponding shift in the global residual land sink; see Table 1). Further, in TRENDY  
12 experiments in which atmospheric CO<sub>2</sub> and climate drivers are varied, the shift appears to  
13 be masked by an increasing trend in NPP associated largely with the CO<sub>2</sub> fertilization  
14 effect (Fig. 3, Fig. S6 and Table S1 in the Supplement). In fact, the high NPP sensitivity  
15 to changes in atmospheric CO<sub>2</sub> concentrations in many of the current generation of  
16 terrestrial biosphere models (Arora et al., 2013) and the potential role of nutrient  
17 limitations (Zaehle, 2013) and/or climate feedbacks (Smith et al., 2015) in mitigating this  
18 sensitivity is presently a subject of intense research.

19

### 20 **3.4 Shifts in R<sub>h</sub> and NEP**

21 In how far the identified climate-driven regime shifts in NPP in the late 1980s translate  
22 into a sustained carbon sink (consistent with the shift seen in the residual land carbon  
23 sink from the GCB; Table 1) depends in part on associated responses in key carbon loss

1 fluxes such as  $R_h$  which (apart from its dependence on substrate supply from NPP) often  
2 depends on climatic factors in a similar fashion as NPP (Lucht et al., 2002). A limitation,  
3 however, is that currently no data-driven analog for  $R_h$  estimation exists and one has to  
4 revert to alternative methods including more uncertain process-based simulations.  
5 Nevertheless to estimate the degree at which shifts in NPP may be potentially offset by  
6 corresponding shifts in  $R_h$  we apply our change point framework also on the  $R_h$  as well as  
7 NEP fluxes from the CASA and TRENDY simulations (see Section 2). Results show that  
8 for the large land regions of interest regime shifts in NPP are repeatedly accompanied by  
9 substantial shifts in  $R_h$  (Table 1, Tables S1-S2 and Figs S2, S5-S6 in the Supplement)  
10 often with 1-2 year lags (seen most clearly when ENSO and volcanic influences are  
11 accounted for). A consequence is that corresponding shifts in NEP are often less robust or  
12 not detectable (Table 1 and Table S3 in the Supplement). For example, in the case of the  
13 two focal regions northern Eurasia and northern Africa, the late 1980s shifts in data-  
14 driven NPP are offset by corresponding shifts in  $R_h$  at levels of 64-66% and 80-90%  
15 (depending on statistical treatment), respectively (Table 1). As stated, the estimated shifts  
16 in the  $R_h$  fluxes are more uncertain and may represent more upper bound estimates as a  
17 new study suggests that carbon models have a tendency to transfer carbon too quickly  
18 through the plant-soil systems because of severe biases in simulated soil carbon and/or  
19 too high  $R_h$  sensitivities to climate (Carvalhais et al., 2014).

20 At global scale, a shift in  $R_h$  can also be estimated as the residual between a NPP  
21 shift and a corresponding shift in the residual land sink based on the GCB (Anderegg et  
22 al., 2015). Using methods that include such residual calculations as well as our direct  
23 model estimates (see Methods in the Supplement), we estimate a shift in global NPP in

1 the late 1980s of  $1.14 \pm 0.34 \text{ PgC yr}^{-1}$  and a corresponding shift in  $R_h$  of  $0.36 \pm 0.48 \text{ PgC}$   
2  $\text{yr}^{-1}$ . Our best estimate for an associated global shift in NEP is  $0.63 \pm 0.30 \text{ PgC yr}^{-1}$  that  
3 amounts to roughly 60% of the magnitude of the late 1980s shift in the residual land sink  
4 from the GCB ( $1.12 \pm 0.14 \text{ PgC yr}^{-1}$ ; based on the three estimates shown in Table 1).

5

#### 6 **4 Discussion**

7 Our findings provide independent evidence from a biospheric modeling perspective for  
8 the abrupt strengthening of the ‘residual’ land carbon sink in the late 1980s (Sarmiento et  
9 al. 2010) and suggest that the underlying driver is a shift in global NPP in response to  
10 coordinated large-scale climate shifts. However, the late 1980s climate perturbations may  
11 also substantially influence fire regimes, but the paucity of data on burned area and  
12 related carbon emissions extending back to the early 80s severely limits estimating  
13 corresponding impacts. For northern Eurasia (which is responsible for the largest  
14 contribution to the late 1980s regime shift in data-driven NPP), however, it is not  
15 anticipated that the observed profound spring warming and greening (inferred through  
16 fAPAR) in the late 1980s may have lead to substantial changes in fire emissions since the  
17 fire activity peaks later in the season (van der Werf et al., 2006). For northern Africa,  
18 changes in fire regimes associated with the late 1980s shift towards wetter conditions  
19 may have a substantial influence on net carbon balance albeit with uncertain direction  
20 since a shift towards wetter conditions may increase (more fuel load) or reduce  
21 (shortening the dry season) fire emissions (Andela and van der Werf, 2014). Models that  
22 can potentially quantify this influence are still in their early phase of development. While  
23 much uncertainty (specifically pertaining to magnitude) remains in estimating the

1 contribution of climate-driven changes in the major land carbon fluxes to the late 1980s  
2 regime shift in the land carbon sink, our regional NPP attributions are consistent with a  
3 reported decrease in the interhemispheric gradient in atmospheric CO<sub>2</sub> in the 1990s  
4 relative to the 1980s that is attributed to an increase in the northern carbon sink (Wang et  
5 al., 2013).

6 Other factors not related to climate may have also played a role in the late 1980s  
7 regime shift of the land carbon sink. A potential large contribution in this regard may be  
8 from land-use and land cover changes across northern Eurasia through agricultural  
9 abandonment and rapid changes in forest management in the aftermath of the late 1980s  
10 post-Soviet collapse. While such processes are accounted for in net LUC emission  
11 estimates compiled in the GCB (and therefore included in our analysis; see Table 1)  
12 corresponding effects may not be fully captured due to a lack of robust data especially in  
13 the period prior the Soviet collapse (Achard et al., 2006). However, at least in the case of  
14 agricultural abandonment newly available estimates (Schierhorn et al., 2013) of  
15 associated carbon sinks for the post-Soviet period 1990-2009 suggest a minor  
16 contribution ( $\sim 0.03 \text{ PgC yr}^{-1}$ ).

17 A remarkable finding is that two key climatic constraints on plant growth  
18 (temperature and precipitation) have shifted in the late 1980s in a way as to facilitate an  
19 abrupt and sustained increase in continental-scale terrestrial NPP. This bears the question  
20 if there is an underlying link that would explain why these large-scale climate pattern  
21 varied nearly synchronously. The Arctic Oscillation (AO) is the most important climate  
22 mode in the northern extratropics (Thompson and Wallace, 1998) and also a prominent  
23 mode in coupled global (Los et al., 2001) and hemispheric (Buermann et al., 2003)

1 climate and satellite vegetation greenness data. Consistent with these results, we find that  
2 over the satellite period 1982-2011 the winter AO is tightly correlated with northern  
3 Eurasian spring temperatures ( $r=0.60$ ,  $P<0.001$ ) and spring fAPAR ( $r=0.40$ ,  $P=0.03$ ),  
4 respectively (Fig. 4). In the late 1980s, the AO together with its regional manifestation  
5 the North Atlantic Oscillation (NAO) (Hurrell, 1995) underwent an extreme shift into  
6 their respective positive phases, thereby moving North Atlantic winter storm tracks  
7 northward and enabling advection of mild maritime air deep into the northern Eurasian  
8 land mass (Thompson and Wallace, 1998). Our results show that the northern Eurasian  
9 biomes responded rapidly to the associated substantial spring warming as evidenced  
10 through synchronous increases in satellite-based vegetation activity (Fig. 4a). Change  
11 point analysis on these drivers of NPP also confirms the existence of this prominent late-  
12 1980s shift (showing significant shifts in winter (JFM) AO (1989,  $p=0.07$ ), Northern  
13 Eurasian spring temperature (1989,  $p<0.001$ ) and Northern Eurasian spring fAPAR  
14 (1990,  $p<0.001$ ), respectively). In the aftermath of this shift, however, spring  
15 temperatures and vegetation activity stayed at elevated levels (causing a sustained impact  
16 on plant carbon uptake; see Fig. 2a) while the AO/NAO exhibited a negative trend, a fact  
17 that may be explained by a more gradual warming response to greenhouse gas forcing  
18 that is superimposed on the more oscillatory influence of the AO/NAO.

19 Northern African wet season rainfall pattern are strongly influenced by Atlantic  
20 sea surface temperature (SST) variability (Hoerling et al., 2006). In this regard, the  
21 warming of the North Atlantic relative to the South Atlantic that resumed in the late  
22 1980s to mid 1990s caused a northward displacement of the Atlantic intertropical  
23 convergence zone (ITCZ) and increased rainfall rates across northern Africa, which led to

1 a recovery from earlier severe drought conditions (Hoerling et al., 2006). This increased  
2 moisture supply also led to rapid increases in satellite fAPAR (Fig. 4b). An open question  
3 is to what extent AO/NAO and Atlantic SST forcings may have interacted (Xie and  
4 Carton, 2004) in the wake of the apparent coordinated regional climate shifts over  
5 northern Eurasia and northern Africa in the late 1980s. It is well established that ENSO  
6 (van der Werf et al., 2004) and volcanic eruptions (Lucht et al., 2002) have a dominant  
7 influence on the terrestrial carbon cycle at interannual time scales and much of recent  
8 research has focused on associated links (Cox et al., 2013; Wang et al., 2014). Our  
9 findings here may suggest that North Atlantic climate variability and corresponding  
10 impacts on adjacent vast land masses may be more important in regards to abrupt,  
11 substantial and more sustained shifts in the terrestrial carbon cycle.

12

## 13 **5 Conclusions**

14 Our results point to a mechanism whereby North Atlantic climate variability modulates  
15 the global terrestrial carbon cycle. New research suggests that a large portion of the  
16 variability in the North Atlantic may be externally forced by anthropogenic aerosols  
17 (Booth et al., 2012) and the pronounced warming trend in the Arctic regions, known as  
18 Arctic amplification (Cohen et al., 2014). Arctic amplification specifically is thought to  
19 intensify under climate change (Deser et al., 2010) and this may drive the AO/NAO more  
20 into their respective negative phases (Cohen et al., 2014) which, based on our results,  
21 would substantially reduce carbon uptake by terrestrial plants and weaken the land carbon  
22 sink. This illustrates the pressing need for improved knowledge of North Atlantic  
23 climate variability and associated forcing mechanisms in order to more credibly

1 project the evolution of the land carbon sink and carbon cycle climate feedbacks  
2 under climate change.

3

#### 4 **References**

5 Achard, F., et al. Areas of rapid forest cover change in boreal Eurasia. *For. Ecol. Manag.*,  
6 237, 322–334, 2006.

7 Andela, N., & van der Werf, G. R. Recent trends in African fires driven by cropland  
8 expansion and El Nino to La Nina transition. *Nature CC*, 4, 791–795, 2014.

9 Anderegg, W. R. L. et al. Tropical nighttime warming as a dominant driver of variability  
10 in the terrestrial carbon sink. *Proc. Nat. Acad. USA*, doi: 10.1073/pnas.1521479112,  
11 2015.

12 Arora, V. K., et al. Carbon-concentration and carbon-climate feedbacks in CMIP5 earth  
13 system models, *J. Clim.* 26, 5289-5314, 2013.

14 Beaulieu, C., Sarmiento, J. L., Mikaloff Fletcher, S., Chen, J. & Medvigy, D.  
15 Identification and characterization of abrupt changes in the land uptake of carbon.  
16 *Glob. Biogeochem. Cycl.*, 26, GB1007, 2012a.

17 Beaulieu, C., Chen, J. & Sarmiento, J. L. Change-point analysis as a tool to detect abrupt  
18 climate variations. [in special issue: Climate predictions: the influence of nonlinearity  
19 and randomness] *Phil. Trans. R. Soc. A*, 370, 1228-1249, 2012b.

20 Booth, B. B. B., Dunstone, N. J., Halloran, P. R., Andrews, T. & Bellouin, N. Aerosols  
21 implicated as a prime driver of twentieth-century North Atlantic climate variability.  
22 *Nature*, 484, 228-232, 2012.

- 1 Buermann, W., et al. Interannual covariability in Northern Hemisphere air temperatures  
2 and greenness associated with El Niño-Southern Oscillation and the Arctic Oscillation.  
3 *J. Geophys. Res.*, 108, doi:10.1029/2002JD002630, 2003.
- 4 Carvalhais, N., et al. Global covariation of carbon turnover times with climate in  
5 terrestrial ecosystems, *Nature*, 514, 213–217, 2014.
- 6 Ciais, P., et al. in *IPCC Climate Change 2013: The Physical Science Basis*. (eds Stocker,  
7 T. F., et al.) 465–570 (Cambridge University Press, Cambridge).
- 8 Cohen, J., et al. Recent Arctic amplification and extreme mid-latitude weather. *Nature*  
9 *Geosci.*, 7, 627–637, 2014.
- 10 Cox, P. M., et al. Sensitivity of tropical carbon to climate change constrained by carbon  
11 dioxide variability. *Nature*, 494, 341-344, 2013.
- 12 Denman, K. L., et al. in *IPCC Climate Change 2007: The Physical Science Basis* (eds  
13 Solomon, S., et al.) 499–587 (Cambridge University Press, Cambridge).
- 14 Deser, C., Tomas, R., Alexander, M. & Lawrence, D. The seasonal atmospheric response  
15 to projected Arctic sea ice loss in the late twenty-first century. *J. Clim.*, 23, 333–351,  
16 2010.
- 17 Donohue, R. J., Roderick, M. L., McVicar, T. R. & Farquhar, G. D. CO<sub>2</sub> fertilisation has  
18 increased maximum foliage cover across the globe’s warm, arid environments.  
19 *Geophys. Res. Lett.*, 40, 3031–3035, 2013.
- 20 Enfield, D. B., Mestas-Nunez, A. M. & Trimble, P. J. The Atlantic Multidecadal  
21 Oscillation and its relationship to rainfall and river flows in the continental U.S.  
22 *Geophys. Res. Lett.*, 28, 2077-2080, 2001.

1 Forkel, M., Migliavacca, M., Thonicke, K., Reichstein, M., Schaphoff, S., Weber, U. and  
2 Carvalhais, N.: Codominant water control on global interannual variability and trends  
3 in land surface phenology and greenness, *Glob. Change Biol.*, 21, 3414–3435, 2015.

4 Greve, P., et al. Global assessment of trends in wetting and drying over land. *Nature*  
5 *Geosci.*, doi:10.1038/ngeo2247, 2014.

6 Hoerling, M. J., Hurrell, J., Eischeid, J. & Phillips, A. Detection and attribution of 20th  
7 century Northern and Southern African rainfall change. *J. Clim.*, 19, 3989–4008,  
8 2006.

9 Harris, I., Jones, P. D., Osborn, T. J. & Lister, D. H. Updated high-resolution grids of  
10 monthly climate observations – the CRU TS3.10 dataset. *Int. J. Climatol.*, 34, 623–  
11 642, 2014.

12 Hurrell, J. W. Decadal trends in the North Atlantic oscillation regional temperatures and  
13 precipitation. *Science*, 269, 676–679, 1995.

14 IPCC. *Climate Change 2013: The Physical Science Basis: Summary for Policymakers.*  
15 (eds Stocker, T. F. et al.) (Cambridge University Press, Cambridge).

16 Kurz, W. A., et al. Mountain pine beetle and forest carbon feedback to climate change.  
17 *Nature*, 452, 987–990, 2008.

18 Le Quéré, C., et al. Trends in the sources and sinks of carbon dioxide, *Nature Geosci.*, 2,  
19 831–836, 2009.

20 Le Quéré, C., et al. The global carbon budget 1959–2011. *Earth Syst. Sci. Data*, 5, 1107–  
21 1157, 2013.

22 Los, S. O., et al. Global interannual variations in sea surface temperature and land surface  
23 vegetation, air temperature, and precipitation, *J. Clim.*, 14, 1535–1550, 2001.

- 1 Los, S. (2013). Analysis of trends in fused AVHRR and MODIS NDVI data for 1982-  
2 2006: Indication for a CO<sub>2</sub> fertilization effect in global vegetation. *Glob. Biogeochem.*  
3 *Cycl.*, 27, 318-330, 2013.
- 4 Lucht, W., et al. Climatic control of the high-latitude vegetation greening trend and  
5 Pinatubo effect. *Science*, 296, 1687-1688, 2002.
- 6 Luysaert, S., et al. CO<sub>2</sub> balance of boreal, temperate, and tropical forests derived from a  
7 global database. *Glob. Change Biol.*, 13, 2509–2537, 2007.
- 8 Piao, S., et al. Changes in satellite-derived vegetation growth trend in temperate and  
9 boreal Eurasia from 1982 to 2006. *Glob. Change Biol.*, 17, 3228–3239, 2011.
- 10 Piao, S., et al. Evaluation of terrestrial carbon cycle models for their response to climate  
11 variability and to CO<sub>2</sub> trends, *Glob. Change Biol.*, 19, 2117–2132, 2013.
- 12 Raczka, B. M., et al. Evaluation of continental carbon cycle simulations with North  
13 American flux tower observations, *Ecol. Monographs*, 83, 531–556, 2013.
- 14 Richardson, A. D., Influence of spring and autumn phenological transitions on forest  
15 ecosystem productivity, *Phil. Trans. R. Soc. B*, 365, 3227-3246, 2010.
- 16 Sarmiento, J. L. et al. Trends and regional distributions of land and ocean sinks.  
17 *Biogeosciences*, 7, 2351–2367, 2010.
- 18 Schierhorn, F., et al. Post-Soviet cropland abandonment and carbon sequestration in  
19 European Russia, Ukraine, and Belarus. *Glob. Biogeochem. Cycl.*, 27, 1175-1185,  
20 2013.
- 21 Sitch, S. et al. Recent trends and drivers of regional sources and sinks of carbon dioxide.  
22 *Biogeosciences*, 12, 653–679, 2015.

1 Smith, W. K. et al. Large divergence of satellite and Earth system model estimates of  
2 global terrestrial CO<sub>2</sub> fertilization, *Nature Clim. Change*, doi:10.1038/nclimate2879.

3 Thompson, D. W. J. & Wallace, J. M. The Arctic oscillation signature in the wintertime  
4 geopotential height and temperature fields. *Geophys. Res. Lett.*, 25, 1297–1300, 1998.

5 van der Werf, G. R., et al. Continental-scale partitioning of fire emissions during the  
6 1997 to 2001 El Nino/La Nina period. *Science*, 303, 73-76, 2004.

7 van der Werf, G. R., et al. Interannual variability in global biomass burning emissions  
8 from 1997 to 2004. *Atm. Chem. Phys.*, 6, 3423–3441, 2006.

9 Wang, Y., Li, M. & Shen, L. Accelerating carbon uptake in the Northern Hemisphere:  
10 evidence from the interhemispheric difference of atmospheric CO<sub>2</sub> concentrations.  
11 *Tellus B*, 65, 20334, 2013.

12 Wang, X., et al. A two-fold increase of carbon cycle sensitivity to tropical temperature  
13 variations. *Nature*, 506, 212-215, 2014.

14 Wild, M. Global dimming and brightening: A review. *J. Geophys. Res.*, 114, D00D16,  
15 2009.

16 Xie, S. P. & Carton, J. A. Tropical Atlantic variability: Patterns, mechanisms, and  
17 impacts. *Earth's Climate*, 121-142, 2004.

18 Zaehle, S. Terrestrial nitrogen–carbon cycle interactions at the global scale. *Phil. Trans.*  
19 *R. Soc. B*, 368, 20130125, 2013.

20 Zhao, M. & Running, S. W. Drought-induced reduction in global terrestrial net primary  
21 production from 2000 through 2009, *Science*, 329, 940–943, 2010.

22 Zhu, Z., et al. Global data sets of vegetation Leaf Area Index (LAI) 3g and Fraction Of  
23 Photosynthetically Active Radiation (FPAR) 3g derived from Global Inventory

1 Modeling and Mapping Studies (GIMMS) Normalized Difference Vegetation Index  
2 (NDVI3g) for the period 1981 to 2011. *Rem. Sens.*, 5, 927–948, 2013.

3

#### 4 **Acknowledgements**

5 We gratefully acknowledge support for this study from the National Aeronautics and  
6 Space Administration Carbon Cycle Science Program (grant NNX11AD45G).

7 We also thank Emanuel Gloor, Stephen Sitch, and John Chiang for constructive  
8 comments that improved the manuscript. Finally, we thank the TRENDY modelling  
9 group for making their data available.

10

#### 11 **Author Contributions**

12 W.B., C.B., B.P. and G.J.C. designed the analyses. W.B., C.B. and B.P. conducted the  
13 analyses. All authors contributed to the writing of the manuscript.

14

#### 15 **Competing financial interests**

16 The authors declare no competing financial interests.

1 **Table 1. Timing and magnitude of abrupt changes in the terrestrial carbon cycle at**  
2 **global and continental scales.** Timing of abrupt change (first data entry) as well as  
3 corresponding direction and magnitude (second data entry in units of PgC yr<sup>-1</sup>) and *P*-  
4 values (in brackets; estimated through Monte Carlo simulations) are provided if a ‘shift in  
5 the mean’ model fits the respective time series best (see Section 2). The timing of a shift  
6 indicates the first year of a new regime. Shifts that are statistically significant ( $P < 0.05$ )  
7 are highlighted in bold. Additional tests were carried out for assessing the nature and  
8 robustness of the shifts including accounting for influences related to ENSO and volcanic  
9 eruptions (Covariates), and specifically removing the two years of largest impact of the  
10 strong Mt. Pinatubo volcanic eruption in the original time series (No Pinatubo). Plots of  
11 all time series analyzed are also provided (Figs S2-S3 in the Supplement).  
12

1

Region	Original data	Covariates <sup>f</sup>	No Pinatubo <sup>g</sup>
<i>Global Carbon Budget 1959-2011</i>			
Residual land sink <sup>e</sup>	<b>1989, +1.03 (0.003)</b>	<b>1989, +1.28 (&lt;0.001)</b>	<b>1989, +1.06 (0.003)</b>
Net land uptake <sup>e</sup>	<b>1989, +1.19 (0.004)</b>	<b>1989, +1.43 (&lt;0.001)</b>	<b>1989, +1.23 (0.001)</b>
<i>Data-driven (CASA) NPP 1982-2011</i>			
Global	1995, +1.18 (0.239) <sup>c</sup>	1989, +1.12 (0.124) <sup>c</sup>	1989, +1.49 (0.084) <sup>c</sup>
Northern land (>30°N)	<b>1988, +0.72 (0.010)<sup>c</sup></b>	<b>1989, +0.62 (0.008)<sup>c</sup></b>	<b>1988, +0.76 (0.003)<sup>c</sup></b>
Tropic./south. land (<30°N)	1995, +0.73 (0.266) <sup>c</sup>	1989, +0.50 (0.526)	1995, +0.70 (0.388) <sup>c</sup>
Northern Eurasia	<b>1988, +0.53 (&lt;0.001)<sup>b</sup></b>	<b>1989, +0.45 (0.001)</b>	<b>1988, +0.54 (&lt;0.001)<sup>b</sup></b>
Northern Africa	<b>1989, +0.20 (0.005)</b>	<b>1989, +0.17 (0.003)</b>	<b>1989, +0.21 (0.001)</b>
<i>Process-based (CASA) R<sub>h</sub> 1982-2011</i>			
Global	<b>1996, +0.96 (0.001)</b>	<b>1990, +0.80 (0.028)<sup>c</sup></b>	<b>1996, +0.94 (0.001)</b>
Northern land (>30°N)	<b>1990, +0.44 (0.003)<sup>c</sup></b>	<b>1990, +0.42 (&lt;0.001)<sup>a,c</sup></b>	<b>1990, +0.46 (&lt;0.001)<sup>c</sup></b>
Tropic./south. land (<30°N)	<b>1996, +0.63 (0.003)</b>	1996, +0.49 (0.054)	<b>1996, +0.61 (0.002)</b>
Northern Eurasia	<b>1988, +0.35 (0.004)<sup>a,c</sup></b>	<b>1990, +0.29 (0.004)<sup>b,c</sup></b>	<b>1988, +0.37 (&lt;0.001)<sup>a,c</sup></b>
Northern Africa	<b>1988, +0.18 (&lt;0.001)</b>	<b>1991, +0.14 (0.003)<sup>b</sup></b>	<b>1988, +0.19 (&lt;0.001)</b>
<i>Process-based (CASA) NEP 1982-2011</i>			
Global	1987 <sup>d</sup>	1999, -0.68 (0.122)	1987 <sup>d</sup>
Northern land (>30°N)	1987, +0.30 (0.318)	1989 <sup>d</sup>	1987, +0.31 (0.304)
Tropic./south. land (<30°N)	1999 <sup>d</sup>	1999, -0.56 (0.087)	1999 <sup>d</sup>
Northern Eurasia	1988, +0.18 (0.061)	1989, +0.15 (0.154) <sup>b,c</sup>	1988, +0.18 (0.074)
Northern Africa	1992 <sup>d</sup>	2003 <sup>d</sup>	1992 <sup>d</sup>

2 a. Not normally distributed (Lilliefors test, 5% critical level)

3 b. Variance not constant (F-test, 5% critical level)

4 c. Residuals not independent (Kruskal-Wallis, 5% critical level)

5 d. 'Linear trend' or 'constant mean' model fits data better than a 'shift in the mean' model

6 d. In the global carbon budget (Le Quéré et al., 2013), the net land uptake is estimated as the difference

7 between global fossil fuel emissions and the sum of atmospheric CO<sub>2</sub> growth rate and oceanic uptake,

8 while the residual land sink is the difference between net land uptake and LUC emissions

9 e. Variability related to ENSO and volcanoes were removed in the original time series through regressions

10 against the multivariate ENSO index and stratospheric optical thickness after Beaulieu et al. (2012a)

11 f. The two Pinatubo years (1992, 1993) were removed in the original time series prior change point analysis

12

1 **Figure captions**

2 **Figure 1. Spatial pattern of abrupt shifts in data-driven NPP.** Maps show (a) timing  
3 and corresponding (b) direction and magnitude of abrupt shifts in data-driven (CASA)  
4 annual NPP for the satellite period 1982-2011. All robust NPP shifts shown here have  
5 passed the two key statistical criteria: (i) a ‘shift in the mean’ model fits the time series at  
6 each grid point best (evaluated through the Schwarz Information Criterion) and (ii) the  
7 shift is also statistically significant ( $P < 0.05$ ) based on Monte Carlo simulations that take  
8 into account explicit uncertainties (Section 2). Maps of shifts that passed only the first  
9 criteria are also provided (Fig. S1 in the Supplement). In (a), the focus regions northern  
10 Eurasia (10°W-180°E, 40°N-70°N) and northern Africa (20°W-50°E, 5°N-20°N) are  
11 outlined. The shifts are only assessed for the period 1987-2006, since for robust change  
12 point detection a minimum span of 5 years of data prior and after a shift is required  
13 (Section 2).

14

15 **Figure 2. Temporal changes in continental data-driven NPP.** Panels show annual and  
16 seasonal (CASA-based) NPP anomalies corresponding to the (a) northern Eurasian and  
17 (b) northern African focus regions (see Fig. 1a). All anomalies are relative to 1982-2011.  
18 Shaded contours represent  $1\sigma$  uncertainties that account for biases in model driver data  
19 (Section 2). To understand which factors are mainly responsible for the identified shifts  
20 (see Table 1), we performed factorial NPP simulations in which only one model driver is  
21 varied whereas all others are kept constant (e.g., ‘fAPAR only’ corresponds to NPP  
22 simulations in which only fAPAR was varied, whereas temperature, precipitation and  
23 solar radiation data were kept at their climatological mean values). It should be noted that

1 satellite fAPAR, a proxy for vegetation cover, is often correlated with climate variables  
2 and this places limits on attributing a single model driver to changes in NPP. The first  
3 year of a new regime in annual NPP is outlined (thick dark red vertical lines; see Table 1)  
4 and the means in NPP anomalies prior and after the shift are also shown (dashed lines).

5

6 **Figure 3. Temporal changes in continental process-based NPP based on nine**

7 **terrestrial biosphere models.** Panels show annual and seasonal NPP anomalies for the

8 (a) northern Eurasian and (b) North African focus regions, based on ensembles of nine

9 biosphere models that participated in the recent TRENDY model intercomparison study

10 (Sitch et al. 2015). In the annual case, results for two sets of model simulations are

11 shown: one in which climate and CO<sub>2</sub> as model drivers were varied (S2) and another one

12 that only takes into account the effect of climate variations (S2 – S1; see Section 2). All

13 anomalies are relative to the 1982-2010 overlapping satellite era to facilitate comparisons

14 with the data-driven NPP simulations (see Fig. 2). Mean ensembles were formed based

15 on anomalies in the single TRENDY models to emphasize temporal changes in NPP and

16 to suppress uncertainties arising from model differences in magnitudes. Shaded contours

17 represent 1 $\sigma$  uncertainties corresponding to the spread in the single TRENDY models.

18 The first year of a new regime in annual NPP is outlined (thick dark red vertical lines;

19 Table S1 in the Supplement) and the means in NPP anomalies prior and after the shift are

20 also shown (dashed lines). In panel (b), the last data point for the year 2010 is omitted

21 since tropical rainfall input data for the TRENDY runs were erroneous for that year (S.

22 Sitch, personal communication).

23

1 **Figure 4. Synchronous continental shifts in climate and satellite vegetation data and**  
2 **links to North Atlantic climate variability.** In panel (a), temporal variations in spring  
3 (MAM) temperature and satellite-based vegetation activity (fAPAR) representative of the  
4 northern Eurasian target region are plotted alongside the winter (JFM) Arctic Oscillation  
5 (AO) and North Atlantic Oscillation (NAO) time series. In panel (b), temporal variations  
6 in wet season (May-Oct) precipitation and fAPAR for the northern African target region  
7 are plotted alongside the annual Atlantic Multidecadal Oscillation (AMO) time series.  
8 Plotted are both annual values (thin dotted lines) and a smoothed time series based on a  
9 seven-point binomial filter (thick lines). All time series are standardized anomalies  
10 relative to the satellite period 1982-2011. All climate indices time series are obtained  
11 from *www.esrl.noaa.gov*. Definitions of the AO and NAO are given in Thompson and  
12 Wallace (1998) and Hurrell (1995), respectively. The AMO is a detrended area-weighted  
13 average of North Atlantic SSTs (0°-70°N) (Enfield et al., 2001).

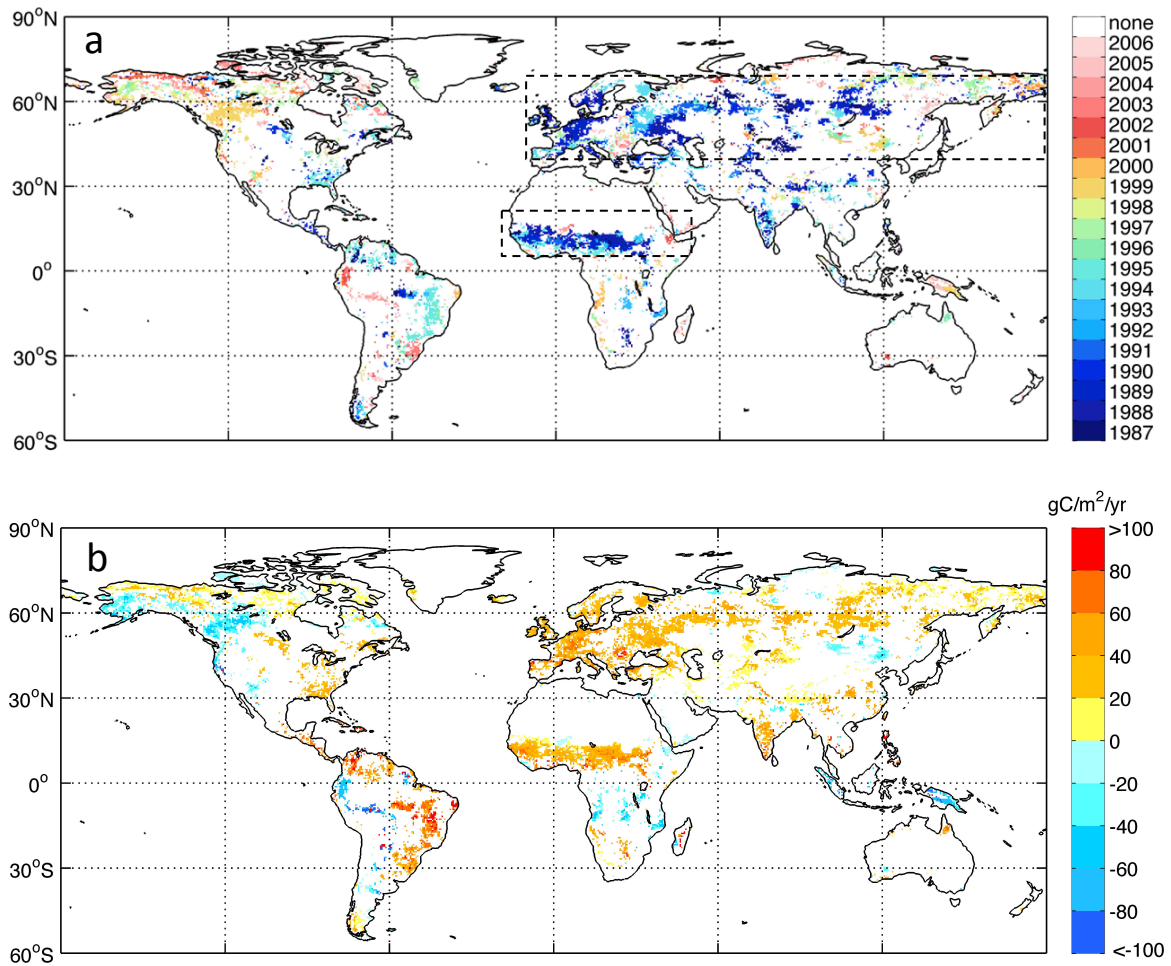


Figure 1

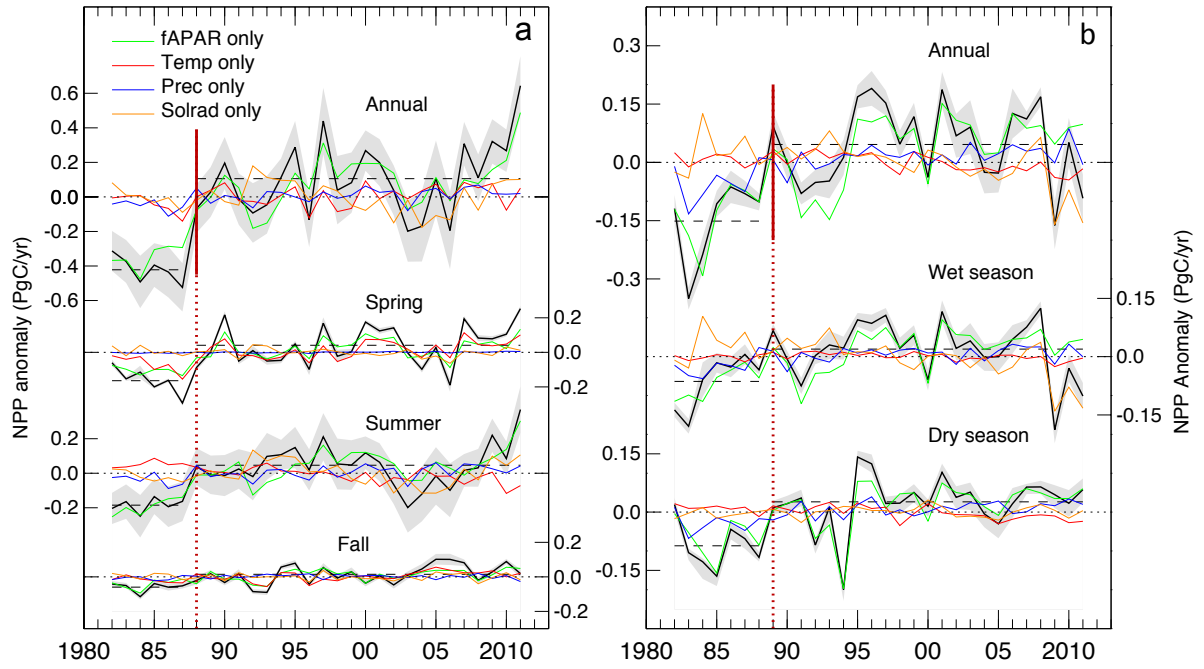


Figure 2

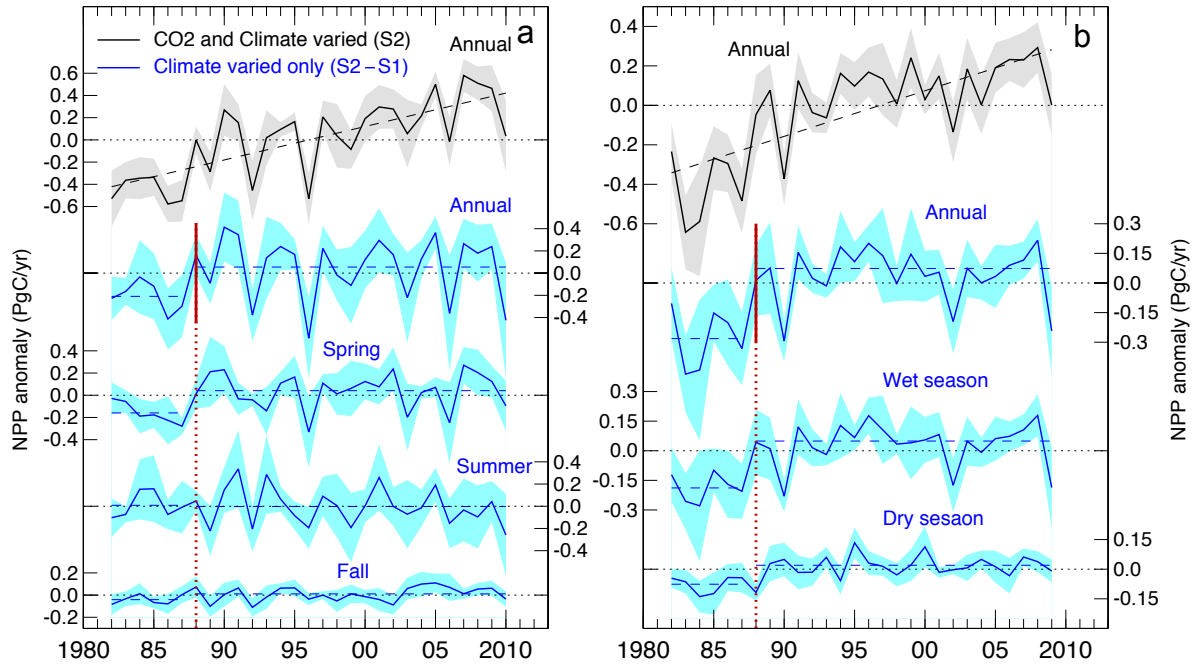


Figure 3

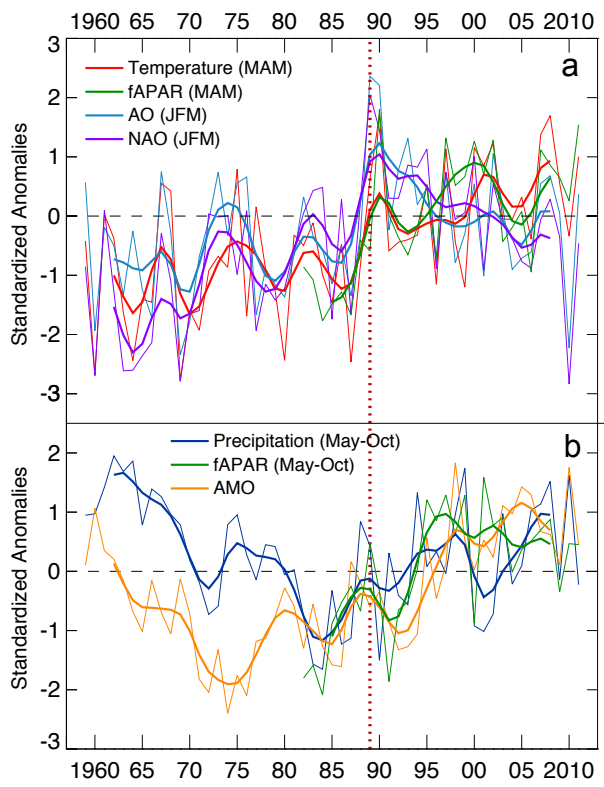


Figure 4